Transition in Domain Morphology of Block Copolymers Undergoing Polymerization

You Iida* and Toshihiro Kawakatsu

Department of Physics, Graduate School of Science, Tohoku University, Sendai 980-8578, Japan

Ryuhei Motokawa, Satoshi Koizumi, and Takeji Hashimoto

Advanced Science Research Center, Japan Atomic Energy Agency, Tokai, Ibaraki 319-1195, Japan

Received September 5, 2008; Revised Manuscript Received October 21, 2008

ABSTRACT: We have studied the dynamics of a morphology transition of domains in a reactive system composed of A−B block copolymer and B monomer, where polymerization occurs at the end of the B subchain of the block copolymer. We propose a new dynamical model for reactive phase separation, where the chain architecture, the chain conformation, and the spatial distribution of the reaction points (reactive chain ends) are taken into account by the use of random phase approximation. Our model is essentially equivalent to the dynamical self-consistent field theory if the system is close to the critical point, but it has an enormous improvement in the computational efficiency. Simulation results show that our modeling is quite useful partially because the inhomogeneity of the spatial distribution of the reactants affects the polymerization and partially because we can perform large-scale and long time simulations because of the high efficiency of our model. We found that as a result of the competition between the phase separation and the polymerization the system shows complex nonequilibrium domain structures that depend on the kinetic pathway of the phase separation and the polymerization.

I. Introduction

Controlling the molecular architecture of the block copolymers is quite important in designing functional devices because the block copolymers show a variety of microphase-separated domain structures depending on their molecular architectures. Thus, many researches have been devoted to clarifying both equilibrium and nonequilibrium microphase-separated domain structures in block copolymer systems provided that block copolymers with certain molecular architectures are given.[1−3]

Few studies have focused on how the existence of the phase-separated domain structures affects the synthesis of the block copolymers. Usual radical polymerization is too fast to study the interplay between the phase separation and the polymerization. However, with the use of the living anionic polymerization or the controlled living radical polymerization techniques,[4−9] one can observe the slow polymerization process under simultaneous phase separation.

As an example, we recently reported an experimental result of a polymer system that undergoes a controlled living radical polymerization (reversible addition−fragmentation chain transfer (RAFT) polymerization) investigated by small-angle neutron scattering (SANS) and gel permeation chromatography (GPC) analyses.[9] In this study, the system is a mixture of poly(methyl methacrylate)-*block*-polystyrene and styrene monomer, where the polymerization occurs at the end of the polystyrene subchain. In this system, we observed a competition between micro- and macrophase separations.[9] We also found that the occurrence of the phase separation decelerates the polymerization.[10]

The main purpose of this work is to propose a coarse-grained model for the dynamics of the micro- and macrophase separation phenomena under the influence of the polymerization. There have been several theoretical attempts to investigate the domain formation processes under chemical reactions by using the time-dependent Ginzburg−Landau (TDGL) model with chemical reaction terms.[11−14] Here the terminology Ginzburg−Landau (GL) means that the free energy of the system is expanded in Taylor series in the density fluctuations and is truncated at a certain order. Such an expansion is usually called the Ginzburg−Landau expansion.[15] These studies are focused on reactions in low-molecular-weight materials where the constituent molecules do not have internal degrees of freedom.

In the case of the polymerization, however, we expect the internal degrees of freedom of the molecules, that is, the chain conformation, to have a considerable effect on the polymerization. There have been very few trials to extend the TDGL model to complex polymeric systems under polymerization. Few examples of such trials were made using the dynamic self-consistent field (SCF) theory.[16,17] In these references, the authors investigate the production of a block copolymer chain by chemically bonding two different homopolymer chains at their ends. Using such dynamical SCF theory, one can take the molecular architecture and the conformation of the constituent polymer chains into account through the path integral calculation. However, because the dynamical SCF technique requires large computer resources, the time and length scales that are accessible with the dynamical SCF simulations are very limited. In the present article, we propose a new model for phase separation under polymerization that demands fewer computer resources than does the dynamical SCF simulations but retains the information on the chain architecture and conformation.

II. Theory

Our target phenomenon is a polymerization process of a mixture of an A−B block copolymer and a B monomer, where phase separation and polymerization of the block copolymer at the end of the B subchain simultaneously take place. This phenomenon was studied using the SANS technique.[9,10] In the previous studies using dynamical SCF theory,[16,17] the chain length was suddenly discontinuously increased by the connection of two homopolymers. On the contrary, in the present model, the degree of polymerization gradually increases because of continuous polymerization at the chain end.

In the real experimental system, it is known that there are many complex factors to this phenomenon such as the polydispersity of the products, the existence of homopolymers as a

* Corresponding author. E-mail: you-i@cmpt.phys.tohoku.ac.jp.

10.1021/ma8020322 CCC: $40.75
Published on Web 11/14/2008

byproduct, the detailed microscopic mechanism of the polymerization, and so on.[10] To focus on the coupling between the phase separation and the polymerization, we drastically simplified the model. Our model is a combination of the TDGL-type model of the reacting system[11−14] with a simplified free-energy model for mixtures of polymers and block copolymers using the GL expansion coupled to the random phase approximation (hereafter we call this model GL-RPA).[18,19] Such a free-energy model based on GL expansion and the RPA is an approximation of the free energy calculated by the SCF theory.[15] However, the GL-RPA free energy converges to that of the SCF theory if the system is close to the critical point of the phase separation, and the GL-RPA model retains the essential properties of the system even outside this critical region as long as another phase transition does not take place. The main advantage of our model compared with the dynamical SCF theory is its much lower demand on computer resources.

To describe our target phenomena, we introduce the local volume fractions of the A subchain, the B subchain, and the B monomers, where the reactive chain end is regarded as a part of the B subchain. Then, the time evolution of this system is assumed to obey the following TDGL-type equation with a reaction term

$$\frac{\partial \phi_K(r,t)}{\partial t} = \nabla L_{\mathrm{K}}\left[\phi_K(r,t)\nabla\frac{\delta F}{\delta \phi_K}\right] + \left.\frac{\partial \phi_K(r,t)}{\partial t}\right|_{\mathrm{react}} \quad (1)$$

where $\phi_K(r, t)$ is the volume fraction of the K-type segments (K = A, B, or m (monomer)) at position r at time t and F is the Helmholtz free energy of the system. The coefficient L_{K} in the right-hand side of eq 1 is the kinetic coefficient. We can assume it to be unity by choosing appropriate units of time t_0 and length l_0. Here, for simplicity, we assumed that the kinetic constants L_{A} and L_{B} are equal. This special choice is justified when we choose the sizes of the A segment and the B segment to be equal because L_{A} and L_{B} are the kinetic coefficients of an A segment and a B segment.[20]

When we take the polymerization process into account in the above TDGL model, we need to introduce another variable, that is, the distribution of the reactive chain end that is denoted as ϕ_{end}. Using this variable, the second term on the right-hand side of eq 1 is given by

$$\left.\frac{\partial \phi_{\mathrm{B}}(r,t)}{\partial t}\right|_{\mathrm{react}} = k\phi_{\mathrm{end}}(r,t)\phi_{\mathrm{m}}(r,t) \quad (2)$$

$$\left.\frac{\partial \phi_{\mathrm{m}}(r,t)}{\partial t}\right|_{\mathrm{react}} = -k\phi_{\mathrm{end}}(r,t)\phi_{\mathrm{m}}(r,t) \quad (3)$$

where k is the reaction constant that is nondimensionalized using the unit time t_0.

The polymeric nature is taken into account through the model free energy F. The explicit expression of this free energy F can be obtained either by the SCF theory or by a more simplified model using the GL-RPA.[15] Here we adopt the latter approach, which is basically the same as that used by Raviv and Wang.[19] In this approach, the free-energy functional is expanded in a functional Taylor series in the spatial fluctuation of the volume fraction $\delta\phi_K(r, t) \equiv \phi_K(r, t) - \bar{\phi}_K$, where $\bar{\phi}_K$ is the spatial average of the volume fraction of the K species. The coefficient of the second-order term in this expansion is accurately calculated using the RPA,[1] whereas the higher order terms are approximated by the corresponding terms in the expansion of the Flory−Huggins mixing entropy. Then, the free energy is given by

$$F[\{\delta\phi_K(r,t)\}] = \frac{1}{2!}\sum_{K,K'}\int \mathrm{d}r\,\mathrm{d}r'\,\Gamma_{KK'}(r,r')\,\delta\phi_K(r,t)\,\delta\phi_{K'}(r',t) + \sum_K \int \mathrm{d}r\,\frac{1}{N_K}\left\{(\bar{\phi}_K+\delta\phi_K(r,t))\log(\bar{\phi}_K+\delta\phi_K(r,t)) - \bar{\phi}_K\log\bar{\phi}_K - \frac{(\delta\phi_K(r,t))^2}{2\bar{\phi}_K}\right\} \quad (4)$$

where N_K is the total number of segments in the K-type subchain and

$$\Gamma_{KK'}(r,r') = (S^{\mathrm{RPA}})^{-1}_{KK'}(r,r') \quad (5)$$

Here $S^{\mathrm{RPA}}_{KK'}(r, r')$ is the two-point spatial correlation function between K and K' segments calculated using the RPA. In the above expression, we used a notation of the inverse of a function $A_{KK'}(r, r')$ denoted as $A^{-1}_{K,K'}(r, r')$, which is defined by

$$\sum_{K''}\int \mathrm{d}\,r''\,A_{KK''}(r,r'')A^{-1}_{K'',K'}(r'',r') = \phi(r-r')\,\delta_{KK'} \quad (6)$$

Note that we do not take into account the release or absorption of the reaction energy in the free-energy model, eq 4. Because of this reason, the free energy F does not necessarily monotonically decrease in time in our simulations.

When we simulate the dynamics of this model polymerization system, there arises a difficulty associated with little components such as the chain ends. Because the volume fraction of the end segments is very much smaller compared with the other components, this component easily induces a numerical instability in the numerical integration scheme. To suppress such instability by simply adjusting the simulation parameters, we had to use a very small time mesh, which greatly reduces the efficiency of the simulation. To avoid this difficulty, we proposed a method for eliminating the end segment distribution from the TDGL equations. For this purpose, we introduced virtual external fields imposed on the K-type segment at position r' denoted as $u_K(r')$. As was done in the RPA, we assume a linear relationship between this external field $u_K(r')$ and the deviation of the local segment density $\delta\phi_K(r)$.

Although our model system has four components (i.e., K = A, B, end, and m) only three types of virtual external fields are necessary because the end segment is the same chemical species as the B segments in the B subchain. Using this property, we can eliminate one of the virtual external fields. In the Fourier space representation, we obtain the following relation:

$$\begin{pmatrix}\delta\psi^4_{\mathrm{A}}\\ \delta\psi^4_{\mathrm{B}}\\ \delta\psi^4_{\mathrm{end}}\\ \delta\psi^4_{\mathrm{m}}\end{pmatrix} = S_4\begin{pmatrix}1&0&0\\0&1&0\\0&1&0\\0&0&1\end{pmatrix}S_3^{-1}\begin{pmatrix}\delta\psi^3_{\mathrm{A}}\\ \delta\psi^3_{\mathrm{B}}\\ \delta\psi^3_{\mathrm{m}}\end{pmatrix} \quad (7)$$

where $\delta\psi_K(q)$ is the Fourier transform of $\delta\phi_K(r)$, $S_3(q)$ is the correlation function matrix for the three-component system composed of A, B, and monomer segments, and $S_4(q)$ is the correlation function matrix for the four-component system composed of A, B, end, and monomer segments, respectively. Here we introduced the superscripts 3 and 4 to the segment densities to distinguish the three-component system and the four-component system, and we omitted the arguments q and t for simplicity. Using eq 7, we can calculate the end-segment distribution $\delta\phi^4_{\mathrm{end}}(r, t)$ on the basis of the density profiles of the other three components, A, B, and the monomer. For details of this treatment, readers should refer to the Appendix.

III. Results and Discussion

We performed a series of dynamical simulations on a 2D system starting from a uniform mixture of A−B block copolymer and B monomer by changing the value of the reaction constant k.

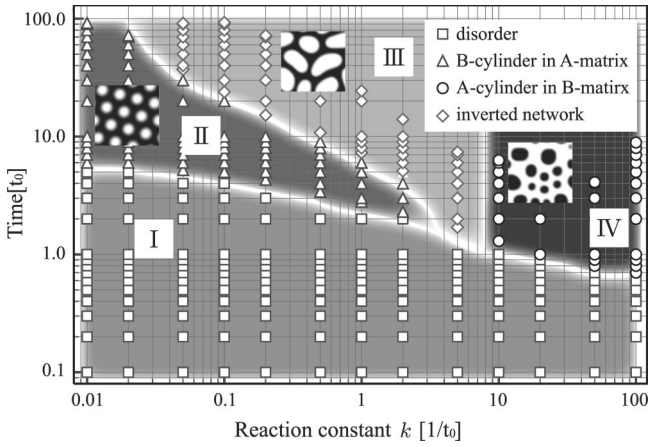

Figure 1. Temporal change of the domain morphology for various values of the reaction constant. A and B domains are shown in black and white, respectively.

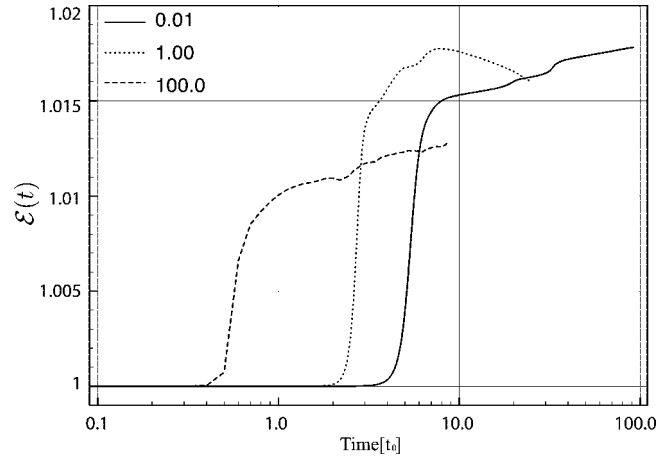

Figure 2. Enhanced reaction rates for the simulations in Figure 1 with the reaction constant $k = 0.01$, 1, and 100.

The system is a 2D system composed of 128×128 square mesh with a mesh width of $\Delta x = 0.1$. A periodic boundary condition is imposed on each side. The TDGL equation, eq 1, is numerically integrated using the Euler scheme with time mesh $\Delta t = 5.0 \times 10^{-5}$. The block copolymer is composed of N_A A segments and N_B B segments with the same size of 1.0. We set the initial sizes of these subchains to be $N_A = 10.0$ and $N_B = 5.0$, which means that the initial block ratio $f^{ini} = N_A/(N_A + N_B) = 0.667$. The average volume fraction of the individual component in the initial state is chosen to be $\bar{\phi}_A = 0.333$, $\bar{\phi}_B = 0.167$, and $\bar{\phi}_m = 0.5$, respectively. As the initial values of the local volume fractions of each component, we use independent Gaussian random numbers at each lattice point with a mean value of $\bar{\phi}_K$ and standard deviations of 1% of this mean value. Throughout this work, we choose the χ parameter between A and B segments, denoted as χ_{AB}, to be 2.0, except for some simulations where the value of χ_{AB} is explicitly mentioned. Therefore, the initial value of $\chi_{AB}N$ (N is the total chain length of the block copolymer) is $2.0 \times 15.0 = 30.0$. With this initial block ratio, the initial composition, and the χ parameter, we confirmed that the system generates hexagonally packed cylinder domains of the B phase in the A matrix to be an equilibrium state by performing a TDGL simulation without the polymerization.

We assume that the size of the reaction end of the B subchain is 10^{-6}. (This value does not affect the simulation results as long as it is small compared with the total chain length.) The value of the reaction constant k is changed in the region $0.01 \leq k \leq 100.0$.

In Figure 1, we show the temporal change of the domain morphology for various values of the reaction constant k [$1/t_0$]. In this Figure, boundaries between different regions are determined by the use of the enhanced reaction rate $E(t)$, which is defined as

$$E(t) = \frac{\int \mathrm{d}r\, k\phi_{end}(r,t)\phi_m(r,t)}{\int \mathrm{d}r\, k\bar{\phi}_{end}(t)\bar{\phi}_m(t)} \tag{8}$$

This enhanced reaction rate measures the effect of the density fluctuations on the enhancement of the polymerization rate compared with that in a uniform system.

In Figure 2, we show the time evolution of the enhanced reaction rates for the simulations with $k = 0.01$, 1, and 100 shown in Figure 1. These curves show a steep increase after a characteristic induction time, then reach a maximum, and afterward decay slowly. Judging from the change in the domain morphology, we understand that the steep increase in $E(t)$ takes place at the same time as the onset of the microphase separation. To classify the different regions in Figure 1, we defined the boundaries between region I and the other regions by the time at which $E(t)$ starts to increase. The boundary between regions II and III is defined by the time at which the slope of $E(t)$ changes its sign from positive to negative. Regions III and IV are distinguished according to which component forms cylindrical domains.

We observed three types of microphase separation processes that strongly depend on the reaction constant, as shown in Figure 1. In the case of a large reaction constant ($k \gtrsim 10$), the polymerization is almost completed well before the microphase separation starts. Then, the system behaves as if the system is a quenched melt of a block copolymer with the final block ratio $f^{final} = 0.333$. In this case, the polymers assemble to form A cylinders in the B matrix.

In the case of a small reaction constant ($k \lesssim 10$), an inverted domain structure, that is, B cylinders in the A matrix, is formed. In this case, the reaction is so slow that the final domain structure is strongly affected by the kinetic pathway that the system traced. If the system was always in equilibrium, then the domain morphology should have changed from a B cylinder in A matrix structure to a lamellar structure. However, in the present case, the growth of the cylindrical domains is faster than the order−order transition of the domains. Thus, the system stays in the cylindrical morphology surrounded by the matrix of the minor phase rather than transforming into the equilibrium lamellar morphology. We named this structure "inverted network".

To check the effect of the spatial inhomogeneity, we performed simulations with three types of reaction models: (a) the case in which the polymerization occurs at the chain end (hereafter referred to as chain-end polymerization), (b) the case in which the polymerization occurs at the whole B subchain (referred to as the hypothetical model because it is unrealistic), and (c) the case in which the system is assumed to be always uniform (referred to as the uniform system).

In Figure 3, we show the time dependence of the monomer conversion averaged over the whole system for these three cases. In these simulations, the value of k is set to be 1.0, $\chi_{AB} = 2.667$ (The initial $\chi_{AB}N = 40.0$), and $\Delta t = 5.0 \times 10^{-7}$. The ratio between the values of the monomer conversion for the chain-end polymerization case and the uniform system case is shown by curve d, which shows a rapid increase at around $t = 0.25$ when the microphase separation starts. Here we discuss the origin of the difference between the uniform system case c and the other two cases a and b. Because the density fluctuations are small in the early stage, the effect of the density fluctuations

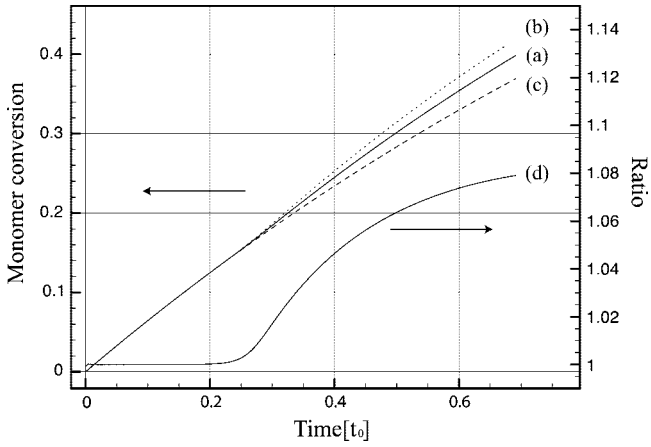

Figure 3. Monomer conversions for (a) the chain-end polymerization, (b) the hypothetical model, and (c) the uniform system. We also plot (d) the ratio between the conversion data for the chain-end polymerization case and the uniform density polymerization case. The initial conditions for the two systems a and b are the same.

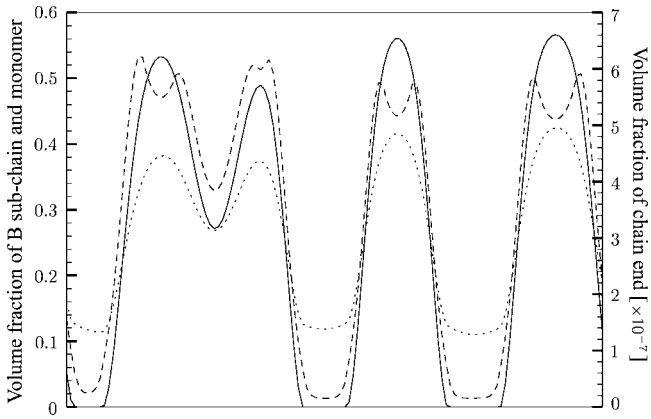

Figure 4. One-dimensional density profiles of the B subchains (−), the chain ends (---), and the monomers (−−−) along a certain line across the system at $t = 0.89t_0$. The scale of the chain-end distribution is enlarged compared with the others.

on the polymerization is negligible in the early stage. In the intermediate to late stages, we find that the monomer conversion for the chain-end polymerization case becomes larger than that in the uniform system case. This difference is induced by the fluctuations in the chain end and the monomer distributions, which increase the product $\phi_{end}\phi_m$ compared with the uniform system case.

The origin of the difference between the two cases a and b is a bit delicate and is affected by the chain conformation. In Figure 4, we plot typical density profiles of the B subchains, the chain ends, and the monomers along a certain line across the system. The scale of the chain-end distribution is enlarged compared with the others to show its functional form clearly. We recognize that the chain-end distribution is broader than that of the B subchain distribution because of the large degrees of freedom of the chain ends. Because the polymerization takes place by a contact between a reaction point (chain end) and a B monomer, the localization of the reaction points accelerates the monomer consumption as a result of the same reason as that discussed above. Thus, the hypothetical model (case b) grows faster than the chain-end polymerization case (case a) and leads to a rapid increase in curve d in Figure 3.

We note that our simulation results show a tendency that is opposite to the experimental behavior;[10] that is, the rate of polymerization is reduced when the phase separation takes place in the experiment. There are several possible reasons for this discrepancy. First, the experimental system has the complication of the macrophase separation as well as of the microphase separation. Such a macrophase separation can affect the monomer composition in the vicinity of the reactive chain ends and may alter the total reaction rate. We should also point out the difference in the strength of the phase separation between the experiments and the simulation, which is measured by the parameter χN. In the experiments,[10] the value of χN is about 100.0, whereas its value in our simulations is chosen to be $\chi N = 50.0$ or 67.8 to suppress instability in the numerical integration scheme. Such a difference may lead to a different way of accumulating the reactants in the domains. Another possibility of the discrepancy is the polydispersity of the block copolymer. However, the GPC measurement showed that the polydispersity of the experimental system is not so large ($M_w/M_n \approx 2.1$) as to affect the polymerization dynamics considerably. The microscopic detail of the polymerization mechanism, such as the many quantum body effects on the reaction process, may also be a possible reason for the discrepancy between the simulation and the experiment. These effects will be taken into account in our future studies.

Self-Consistent Field Simulation. In the previous section, we presented the simulation results of the model that is based on the GL-RPA. As was discussed in the Introduction, the evaluation of the free energy based on the GL-RPA theory is much faster than that based on the SCF theory at the expense of the quantitative accuracy in the evaluation of the chain conformation. Thus, it is important to evaluate how much faster the GL-RPA theory is than the SCF theory. For this purpose, we performed an SCF simulation ($k = 1.0$) with the same parameters and the same system size as the GL-RPA simulations.

The SCF simulation was performed using an enhanced version of SUSHI software in OCTA system provided by T. Honda.[21] Both the GL-RPA simulations and the SCF simulations were performed on a single Opteron CPU (3.0 GHz) machine for comparison.

The simulations were performed on a rather small system with 64×64 meshes with up to 36 000 time steps with $\Delta t = 5 \times 10^{-5}$ (up to $1.8t_0$). For these simulation runs, the SCF simulation took 130 385 s, whereas the GL-RPA simulation took 2873 s. Thus, the GL-RPA method is about 45 times faster than the SCF method. Such an enhancement in the computational efficiency is crucial for performing the long time simulations on large-scale systems as we performed in the present study.

Conclusions

We have studied the effects of the microphase separation on the time evolution of the polymerization process of the B subchain of the A−B block copolymer in B solvent. We observed several types of typical time evolutions of the domain structures, which are strongly dependent on the kinetic pathways that the system traced. Therefore, the final domain structure obtained in this process may be nonequilibrium. An example is the network structure formed by the minor component shown in Figure 1.

We also studied the effect of the spatial distribution of the reaction points. The microphase separation accelerates the polymerization because the reaction points and the monomers are confined to a narrow region in the domains. The consumption of the monomers in the case in which the polymerization takes place at the chain end is less than that in the case in which the polymerization is assumed to take place over the whole B subchain (Figure 3). This is because the distribution of the chain end is broader than that of the whole B subchain because of the larger degrees of freedom of the chain ends.

We also checked the efficiency of our GL-RPA method compared with the dynamical SCF method, which is, in general, more accurate in evaluating the conformation entropy of the chains. The simulation results show that the GL-RPA method is about 45 times faster than the dynamical SCF method. Such efficiency is useful for performing large-scale simulations in the late stage of the phase separation.

Acknowledgment. We thank Dr. Takashi Honda for modifying the SUSHI code so that the polymerization process that corresponds to our simulations could be treated. This work is supported by the Japan Atomic Energy Agency, the 21st century center of excellence program "Exploring new science by bridging particle-matter hierarchy," and a Grant-in-Aid for Scientific Research on Priority Area "Soft Matter Physics" from the Ministry of Education, Culture, Sports, Science, and Technology of Japan.

Appendix

In this Appendix, we show the details of the derivation of eq 7. Following the technique used in RPA, we assume that a deviation of the segment density $\delta\phi(r)$ at position r is induced by a virtual external field imposed at position r', which is denoted as $u(r')$ through the linear relation

$$\delta\phi(r) = -\beta \int \mathrm{d}r'\, S(r - r')u(r') \tag{9}$$

where β is the inverse of $k_\mathrm{B}T$ and $S(r - r')$ is the two-point correlation function of the segment distribution.

By applying this linear relation to our multicomponent system and transforming the results into Fourier space, we obtain the following relation

$$\begin{pmatrix} u_\mathrm{A}(q,t) \\ u_\mathrm{B}(q,t) \\ u_\mathrm{m}(q,t) \end{pmatrix} = -\frac{1}{\beta} S_3^{-1}(q) \begin{pmatrix} \delta\psi_\mathrm{A}^3(q,t) \\ \delta\psi_\mathrm{B}^3(q,t) \\ \delta\psi_\mathrm{m}^3(q,t) \end{pmatrix} \tag{10}$$

where $\delta\psi_K(q)$ is the Fourier component of the local deviation $\delta\phi_K(r)$, $S_3(q)$ is the correlation function between A, B, and monomer segments, and the subscript and superscript 3 denotes that the total density is decomposed into three fields. The virtual external field imposed on the end segments $u_\mathrm{end}(q, t)$ is assumed to be the same as that imposed on the B segments $u_\mathrm{B}(q, t)$ because they are the same chemical species. Thus we obtain

$$\begin{pmatrix} \delta\psi_\mathrm{A}^4(q,t) \\ \delta\psi_\mathrm{B}^4(q,t) \\ \delta\psi_\mathrm{end}^4(q,t) \\ \delta\varphi_m^4(q,t) \end{pmatrix} = -\beta S_4(q) \begin{pmatrix} u_\mathrm{A}(q,t) \\ u_\mathrm{B}(q,t) \\ u_\mathrm{B}(q,t) \\ u_\mathrm{m}(q,t) \end{pmatrix} \tag{11}$$

where $S_4(q)$ is the correlation function between A, B, end, and monomer segments. Here we introduced the subscript and superscript 4 to denote that the total density is decomposed into four fields including the end segment density. By combining eqs 10 and 11 and eliminating the external fields $u_K(q)$, we obtain eq 7.

References and Notes

(1) Leibler, L. *Macromolecules* **1980**, *13*, 1602–1617.
(2) Matsen, M. W.; Schick, M. *Phys. Rev. Lett.* **1994**, *72*, 2660–2663.
(3) Khandpur, A. K.; Förster, S.; Bates, F. S. *Macromolecules* **1995**, *28*, 8796–8806.
(4) Szwarc, M. *Nature* **1956**, *178*, 1168–1169.
(5) Hawker, C. J.; Bosman, A. W.; Harth, E. *Chem. Rev.* **2001**, *101*, 3661–3688.
(6) Kagimoto, M.; Ando, T.; Sawamoto, M. *Chem. Rev* **2001**, *101*, 3689–3746.
(7) Chiefari, J.; Chong, Y. K.; Ercole, F.; Krstina, J.; Jeffery, J.; Le, T. P. T.; Mayadunne, R. T. A.; Meijs, G. F.; Moad, C. L.; Moad, G.; Rizzardo, E.; Thang, S. H. *Macromolecules* **1998**, *31*, 5559–5562.
(8) Rizzardo, E.; Chiefari, J.; Mayadunne, R. T. A. Synthesis of Defined Polymers by Reversible Addition-Fragmentation Chain Transfer: The RAFT Process. In *Controlled/Living Radical Polymerizations Progress in ATRP, NMP, and RAFT*; Matyjaszewki, K., Ed.; American Chemical Society: Washington, DC, 2000; Vol. *768*, pp 278−295.
(9) (a) Motokawa, R.; Iida, Y.; Zhao, Y.; Hashimoto, T.; Koizumi, S. *Polym. J.* **2007**, *39*, 1312–1318. (b) Motokawa, R.; Koizumi, S.; Zhao, Y.; Hashimoto, T. *J. Appl. Crystallogr.* **2007**, *40*, s645–s649.
(10) Motokawa, R.;et al., unpublished.
(11) Glotzer, S. C.; Stauffer, D.; Jan, N. *Phys. Rev. Lett.* **1994**, *72*, 4109–4112.
(12) Christensen, J. J.; Elder, K.; Fogedby, H. C. *Phys. Rev. E* **1996**, *54*, R2212–R2215.
(13) Zhu, Y. J.; Ma, Y.-q. *Phys. Rev. E* **2003**, *67*, 021804.
(14) Zhu, Y.-M. *Phys. Rev. E* **1996**, *54*, 1645–1651.
(15) Kawakatsu, T. *Statistical Physics of Polymers: An Introduction*. Springer: Berlin, 2004.
(16) Maurits, N. M.; Sevink, G. J. A.; Zvelindovsky, A. V.; Fraaije, J. G. E. M. *Macromolecules* **1999**, *32*, 7674–7681.
(17) Honda, T.; Kawakatsu, T.; Doi, M. Proceedings of the International Conference on Advanced Polymers and Processing, Yonezawa, Japan, Oct. 30−Nov. 2, 2001.
(18) Ohta, T.; Motoyama, M.; Ito, A. *J. Phys.: Condens. Matter* **1996**, *8*, A65–A80.
(19) Bohbot-Raviv, Y.; Wang, Z. G. *Phys. Rev. Lett.* **2000**, *85*, 3428–3431.
(20) Furuichi, K.; Nonomura, C.; Kawakatsu, T.; Doi, M. *J. Chem. Phys.* **2002**, *117*, 9959.
(21) Honda, T.; Kodama, H.; Roan, J.-R.; Morita, H.; Urashita, S.; Hasegawa, R.; Yokomizo, K.; Kawakatsu, T., and Doi, M., *SUSHI Users Manual*; OCTA: Nagoya, Japan, 2006. http://octa.jp.

MA8020322